COMMUNICATION

Solvent-Triggered Breakdown of Complete Solid Solution Behaviour Enables Direct Enantioselective Crystallization of a Pharmaceutical Salt.

Received 00th January 20xx,
Accepted 00th January 20xx

DOI: 10.1039/x0xx00000x

Yihua Jiang,[a] Sokhna Souare,[b] Koen Robeyns,[a] Fucheng Leng,[c] Laurent Collard,[a] and Tom Leyssens*[a]

We highlight the role of solvent stoichiometry in chiral resolution of a fully miscible solid solution system of phenprocoumon-quinidine salt. Incorporation of a bis-acetone tunnel solvate selectively stabilizes *S*-phenprocoumon, breaking solid solution behaviour and enabling up to 96:4 ee in a single step.

Enantiomers frequently display different pharmacological profiles, and access to both forms is essential for drug development and regulatory compliance.[1,2] Crystallization-based chiral resolution, including preferential crystallization, diastereomeric salt formation, cocrystal-mediated approaches and Dutch Resolution, remains a central strategy due to ease in scalability and for economic reasons.[3–7] These approaches, however, rely on the presence of resolvable solid phases. Conglomerates allow for direct resolution through preferential crystallization,[5,7–9] while racemic compounds require addition of a secondary chiral agent allowing to position both enantiomers in different multi-component solid phases (eg. a diasteriomeric pair).[10–14]

Solid solutions represent a third possibility for racemates. In these latter, both enantiomers occupy identical crystallographic sites and can substitute each other, either completely or up to a given extent. Solid solutions can occur for the racemate, as well as multi-component systems comprising the target compound. These systems pose challenges during process development, as no (or limited) resolution occurs. When partial solid solution formation occurs, a multi-step crystallization process guided by quasi-ternary phase diagrams, can allow gradual enrichment. For systems showing complete solid solution formation no effective method for separation has yet been reported.[10,15–19]

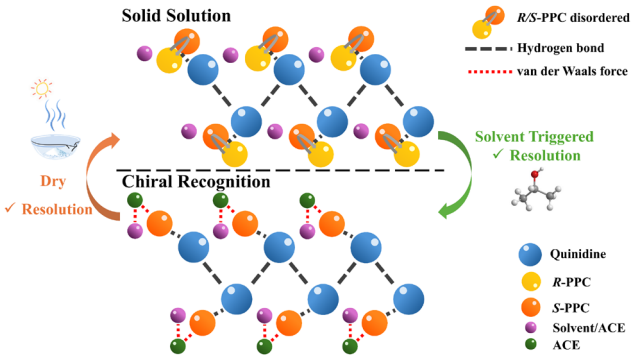

Scheme 1 Schematic Illustration of Solvent-Driven Chiral Recognition in a Solid Solution System of the Salt Composed of phenprocoumon and quinidine.

Phenprocoumon (PPC) is a commonly used oral anticoagulant in several European countries. The *S*-enantiomer exhibits superior pharmacological efficacy.[20–25] The resolution of racemic phenprocoumon (*RS*-PPC) using quinidine was previously reported by Bruce and Karl. The suggested process requires multiple crystallization steps,[26] using mixed solvent systems of chlorofore/acetone, and chloroform/ethanol. As the nature of the solvent was highlighted crucial, and based on our earlier work showing how an achiral solvent can orient the resolution process, we explored this system further.

We, here, highlight how, a mere change in solvent can transform the *RS*-phenprocoumon-quinidine (*RS*-PPC-QD) salt from a solid-solution to an enantioselective system, enabling resolution. This is accomplished by acetone inducing the formation of a unique ~~tunnel~~ solvate incorporating exclusively the *S*-enantiomer, thereby enabling spontaneous resolution up to 96:4 *S*:*R* ratio in a single operation (Scheme 1). Other solvents lead to formation of isostructural *RS*-PPC-QD solvates which show complete solid solution behavior, not-suitable for resolution. We, therefore, here are the first to show how

[a] *Institute of Condensed Matter and Nanosciences, Université catholique de Louvain, 1348 Louvain-La-Neuve, Belgium. E-mail: tom.leyssens@uclouvain.be*
[b] *Univ Rouen Normandie, Normandie Uinv, SMS, UR 3233, F-76000 Rouen, France.*
[c] *Food Science Building, University College Cork, Cork T12 K8AF, Ireland.*
† Electronic Supplementary Information (ESI) available: synthesis, characterization methods, and results. CCDC 2352967-2352968. See DOI: 10.1039/x0xx00000x

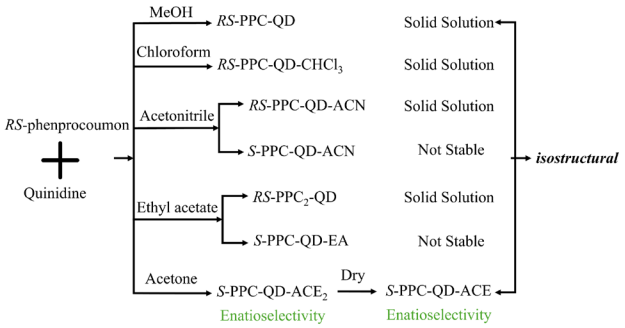

Scheme 2 Systematic Outcomes of Solid Phases from Phenprocoumon–Quinidine Salts in Solvent Screening.

solvate stoichiometry and lattice topology can be used toon break solid solution behavior and enable enantioselective crystallization.

To contextualize this exceptional behaviour, a comprehensive survey of solvates obtained from alcohols, nitriles, halogenated solvents, esters, aromatics, and ethers was conducted. Representative structures, that are exemplified by the *RS*-PPC-QD-ACN solvate, confirmed a consistent supramolecular architecture throughout these systems: zigzag chains of quinidine molecules hydrogen bonded to phenprocoumon, forming X-shaped structural units that pack into layered motifs, with statistical *R*/*S* occupancy at the phenprocoumon site and solid solution behaviour regardless of solvent identity (Fig. 1). Minor variations, such as alternating layer orientation or different solvent-filling of peripheral pockets, did not disrupt the fundamental chain topology, and slurry experiments consistently returned nearly racemic materials (Table 1).

A distinct 2:1 phenprocoumon-rich polymorph (*RS*-PPC$_2$-QD) was also identified. While structurally related through the same chain backbone, this form incorporates an additional phenprocoumon at a site normally occupied by solvent in solvates, producing phenprocoumon-rich layers via aromatic stacking (Fig. S8). Despite the altered stoichiometry and subtle packing differences, this form likewise displayed no chiral discrimination, reinforcing the dominance of solid solution behaviour in most conditions.

Against this backdrop, the exception arose when crystallization was conducted in acetone. Single-crystal diffraction revealed a

Table 1 HPLC resolution results on *RS*-phenprocoumon and quinidine salt in different solvents.

Solvent	Solid Phase	
	S-phenprocoumon	*R*-phenprocoumon
Methanol	50	50
Ethanol	70	30
Acetone	96	4
Acetonitrile	50	50
Ethyl acetate	53	47
Ether	50	50
Dichloromethane	57	43
Tetrahydrofuran	56	44
Toluene	50	50

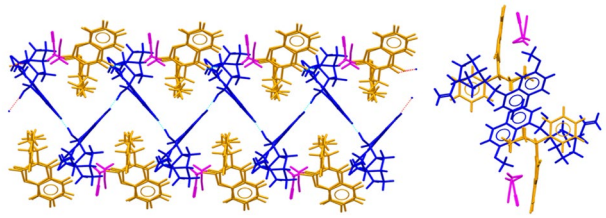

Fig. 1 Typical packing methods of *RS*-PPC-QD solid solutions solid solution, representing by *RS*-PPC-QD-ACN.

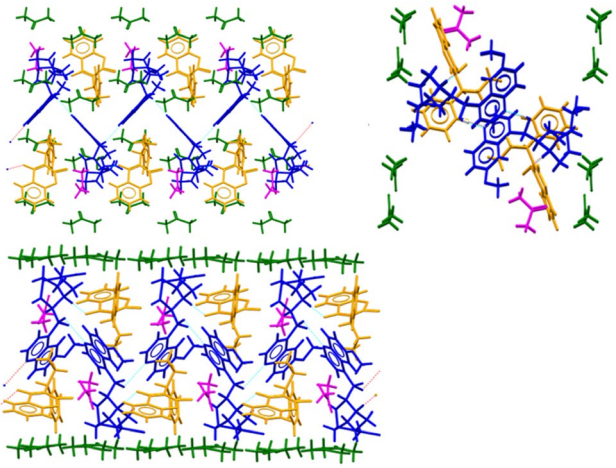

Fig. 2 Similar packing method of *S*-PPC-QD-ACE$_2$ among different directions as solid solution system with the typical zigzag chain and X-shaped motif.

monoclinic $P2_1$ lattice containing two equivalents of acetone per PPC-QD pair (*S*-PPC-QD-ACE$_2$). This structure exhibited strictly parallel alignment of chains, resulting in a more rigid, uniformly oriented framework (Fig. 2). When one acetone in the normal solvent position like other solvates in ACN, EA and $CHCl_3$, the second equivalent of acetone formed a continuous solvent "tunnel" surrounding the chains, creating an asymmetric local environment compatible only with *S*-phenprocoumon. This represents a rare instance where a hydrogen-bonded salt that normally forms a complete solid solution instead crystallizes enantiospecifically due solely to the presence of a second equivalent of solvent. It demonstrates that the second equivalent of acetone is essential for imposing the geometric constraints necessary for chiral recognition.

The structural basis for this enantio-specificity appears to arise from a combination of geometric and energetic effects. The tunnel-like solvation layer sterically restricts the local environment around phenprocoumon, creating a binding pocket whose asymmetry is more compatible with the *S*-enantiomer. *S*-enantiomer was stabilized by weak van der Waals interaction by the layer acetone molecules. This arrangement stabilizes the *S*-enantiomer through a cumulative packing advantage. This subtle but decisive geometric fit cannot be achieved in structures where only one equivalent of solvent is present, explaining why other solvates system lack chiral discrimination.

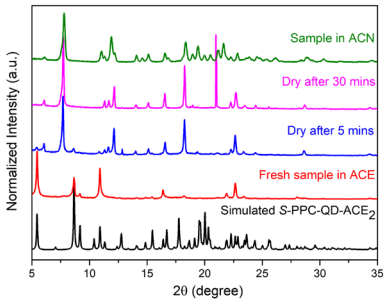

Fig. 3 PXRD patterns of *S*-PPC-QD-ACE$_2$ from simulation and experiments after different treatment, while red one represents the fresh sample in acetone, and blue and purple curves represent fresh samples after keeping at 85°C for 5 mins and 30 mins; and green curve is the simulated PXRD pattern of *RS*-PPC-QD-ACN.

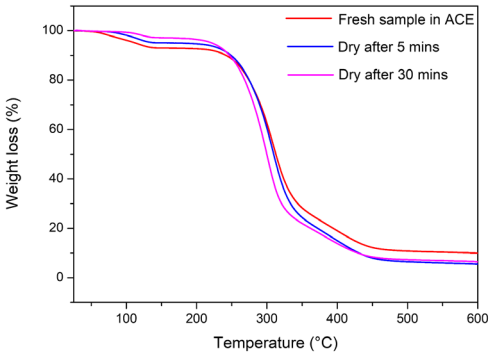

Sample	Weight Loss (%)	Molar equivalent of solvent
Fresh sample in ACE	7.0	0.78
Dry after 5 minutes	4.0	0.50
Dry after 30 minutes	2.7	0.29

Fig. 4 TGA curves of fresh sample of *S*-PPC-QD-ACE$_2$, and then after keeping at 85°C for 5 mins and 30 mins.

The stability and evolution of this acetone-driven lattice were further clarified through solvent-loss experiments. Freshly isolated samples directly from wet slurries exhibited PXRD patterns corresponding to the fully solvated *S*-PPC-QD-ACE$_2$ phase. However, gradual evaporation like heating, drying under ambient conditions, or filtration collapsed the solvent channels, yielding pseudo-1-equivalent acetone solvate with PXRD patterns resembling those of the *RS*-PPC-QD-ACN solid solution solvate motif (Fig. 3 and Fig. S9).

TGA analysis revealed a gradual and well-defined mass-loss process corresponding to the release of acetone molecules from the channels. For the freshly collected *S*-PPC-QD-ACE$_2$ sample, the estimated acetone content was approximately 0.78 equivalents per formula unit, reflecting partial tunnel evaporation during sample transfer and handling. Notably, the 5-min sample after heating at 85°C contains both *S*-PPC-QD-ACE$_2$ and *S*-PPC-QD-ACE phase, which is consistent with the mass-loss of 4.0% (0.5 equivalents acetone) in its TGA trace. In contrast, the 30-min sample corresponds solely to *S*-PPC-QD-ACE, and its TGA curve shows a simpler, single-stage release process with a small weight loss of 2.7%, approaching 0.29 equivalents acetone per single formula unit (Fig. 4).

It is worth emphasizing that the experimentally calculated acetone contents are significantly lower than the theoretical stoichiometries for the corresponding solvates. This discrepancy arises from the high volatility and intrinsic instability of acetone, which allows substantial solvent escape even at room temperature or under minimal handling. Such reduced apparent solvent contents and the associated mass-loss behaviour can be similarly observed for other solid-solution solvate systems (Fig. 4 and Fig. S11-S15).

Despite progressive solvent loss, the PPC-QD system shows a striking propensity to form isostructural solids across a wide range of crystallization conditions. This persistence of a common packing framework indicates that the lattice is inherently biased toward a shared structural motif (Fig S3-S8). Incorporation of additional solvent does not disrupt this architecture.

This mechanism suggests broader implications for resolution strategies in solid-solution-forming systems. Due to lack of enantioselectivity, solid solutions are often considered unsuitable for spontaneous resolution. However, our results demonstrate that solvent molecules, when incorporated in the correct number and spatial arrangement, may impose geometric constraints that modulate the substitutional flexibility of the lattice. In this case, a second equivalent of acetone, which is absent in all other solvates, rigidifies the packing sufficiently to discriminate between enantiomers. Once the enriched lattice is established, subsequent solvent loss produces a structure that is no longer enantioselective in other cases but retains the initial enrichment through kinetic trapping. The emergence of enantiospecific is therefore not an intrinsic property of the molecular pair but of a specific solvated lattice architecture that exists only within a narrow region of stoichiometric and structural space.

An isoplethal ternary phase diagram (*RS*-phenprocoumon, quinidine and acetone) system was constructed for comprehensive understanding of this system. It is cross-section of the full quaternary diagram consisted of *R*-phenprocoumon, *S*-phenprocoumon, quinidine and acetone solvent. For this phase diagram, *RS*-phenprocoumon, quinidine and acetone in different molar ratio were placed in vials for 7 days for equilibrium at 25°C. It confirmed that *S*-PPC-QD-ACE$_2$ is thermodynamically stable across board composition with high chiral resolution from the phase diagram (Fig. 5 and and Table S2).

The *S*-PPC-QD-ACE$_2$ solvate reveals a fundamentally new route to resolving solid solution systems. As far as we know, this work provides the first example where complete solid solution behaviour is broken, resulting in the enantiopure salt by simply forming a specific solvate without disturbing the inherent packing architecture of the solid solution system.

The phenomenology closely parallels, but is distinct from stoichiometry-controlled cocrystal systems, where different cocrystal compositions selectively incorporate different enantiomers. In our case, the stoichiometric variable is the solvent rather than a coformer, and the enantioselectivity arises from a lattice that is structurally accessible only through solvate stabilization. This expands the conceptual toolkit available to crystal engineers by demonstrating that solvent stoichiometry

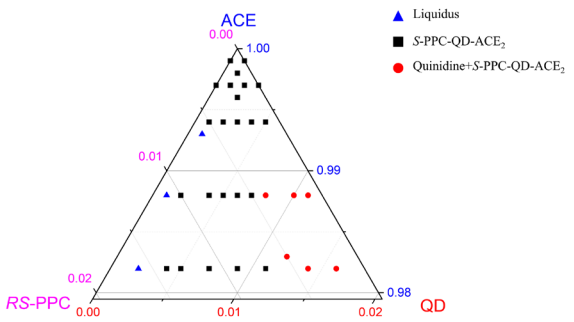

Fig. 5 Isophethal Ternary Phase Diagram of *S*-PPC-QD-ACE_2.

can play the same role as co-former stoichiometry in enabling enantioselective crystallization.

This work demonstrates that carefully tuned solvation can override intrinsic solid solution tendencies and enable spontaneous chiral resolution in systems traditionally deemed unresolvable. The approach should be generalized to other salt or cocrystal systems where solvent-driven lattice architecture may unlock enantioselective crystallization pathways.

Conflicts of interest

There are no conflicts to declare.

Acknowledgements

Author would like to thank the China Scholarship Council (CSC) for financial support.

Notes and references

1 I. Agranat, S. R. Wainschtein and E. Z. Zusman, *Nat Rev Drug Discov*, 2012, **11**, 972–973.
2 S. W. Smith, *Toxicological Sciences*, 2009, **110**, 4–30.
3 C. Rougeot and J. E. Hein, *Org. Process Res. Dev.*, 2015, **19**, 1809–1819.
4 V. Kovalenko and I. Císařová, *Chirality*, 2023, **35**, 1012–1018.
5 F. Zhou, O. Shemchuk, M. D. Charpentier, C. Matheys, L. Collard, J. H. Ter Horst and T. Leyssens, *Angew Chem Int Ed*, 2021, **60**, 20264–20268.
6 R. M. Kellogg, J. W. Nieuwenhuijzen, K. Pouwer, T. R. Vries, Q. B. Broxterman, R. F. P. Grimbergen, B. Kaptein, R. M. La Crois, E. De Wever, K. Zwaagstra and A. C. Van Der Laan, *Synthesis*, 2003, 1626–1638.
7 K. Sakai, N. Hirayama and R. Tamura, Eds., *Novel Optical Resolution Technologies*, Springer Berlin Heidelberg, Berlin, Heidelberg, 2007, vol. 269.
8 A. M. Chen, Y. Wang and R. M. Wenslow, *Org. Process Res. Dev.*, 2008, **12**, 271–281.
9 H. Lorenz, A. Perlberg, D. Sapoundjiev, M. P. Elsner and A. Seidel-Morgenstern, *Chemical Engineering and Processing: Process Intensification*, 2006, **45**, 863–873.
10 S. Songsermsawad, O. Shemchuk, K. Robeyns, F. Zhou, A. E. Flood and T. Leyssens, *Crystal Growth & Design*, 2024, **24**, 2977–2984.
11 L. Pasteur, *Notice sur l'origine de l'acide racémique*, 1853.
12 L. Pasteur, *Transformation des acides tartriques en acide racémique: découverte de l'acide tartrique inactif: nouvelle méthode de séparation de l'acide racémique en acides tartriques droit et gauche*, Mallet-Bachelier, 1853.
13 R. M. Kellogg, in *Advances in Organic Crystal Chemistry: Comprehensive Reviews 2015*, 2015, pp. 421–443.
14 W. Ten Hoeve and H. Wynberg, *J. Org. Chem.*, 1985, **50**, 4508–4514.
15 S. Chen, H. Xi, R. F. Henry, I. Marsden and G. G. Z. Zhang, *CrystEngComm*, 2010, **12**, 1485.
16 M. Balawejder, K. Galan, M. Peter Elsner, A. Seidel-Morgenstern, W. Piatkowski and D. Antos, *Chemical Engineering Science*, 2011, **66**, 5638–5647.
17 H. Kaemmerer, H. Lorenz, S. N. Black and A. Seidel-Morgenstern, *Crystal Growth & Design*, 2009, **9**, 1851–1862.
18 F.-X. Gendron, J. Mahieux, M. Sanselme and G. Coquerel, *Crystal Growth & Design*, 2019, **19**, 4793–4801.
19 R. Oketani, K. Shiohara and I. Hisaki, *Chem. Commun.*, 2023, **59**, 6175–6178.
20 M. Bonduel, G. Sciuccati, M. Hepner, A. F. Torres, G. Pieroni, J. P. Frontroth and R. M. Serviddio, *Journal of Thrombosis and Haemostasis*, 2003, **1**, 1740–1743.
21 J. Hirsh, J. E. Dalen, D. R. Anderson, L. Poller, H. Bussey, J. Ansell, D. Deykin and J. T. Brandt, *Chest*, 1998, **114**, 445S-469S.
22 M. M. Bonduel, *Thrombosis Research*, 2006, **118**, 85–94.
23 A. P. A. Gadisseur, F. J. M. Van Der Meer, H. J. Adriaansen, S. D. Fihn and F. R. Rosendaal, *Br J Haematol*, 2002, **117**, 940–946.
24 E. Jahnchen, T. Meinertz, H.-J. Gilfrich, U. Groth and A. Martini, *Clin Pharma and Therapeutics*, 1976, **20**, 342–349.
25 M. Remko, R. Broer and A. Remková, *RSC Adv.*, 2014, **4**, 8072–8084.
26 B. D. West and K. P. Link, *Journal of Heterocyclic Chem*, 1965, **2**, 93–94.